ELSEVIER

Thermochimica Acta 391 (2002) 227–243

thermochimica acta

www.elsevier.com/locate/tca

Segmental dynamics in poly(oxymethylene) as studied via combined differential scanning calorimetry/creep rate spectroscopy approach

Vladimir A. Bershtein[a,*], L.M. Egorova[a], V.M. Egorov[a], N.N. Peschanskaya[a], P.N. Yakushev[a], M.Y. Keating[b], E.A. Flexman[b], R.J. Kassal[b], K.P. Schodt[b]

[a]*Ioffe Physico-Technical Institute of the Russian Academy of Sciences, 26 Politechnicheskaya Str., 194021 St. Petersburg, Russia*
[b]*E.I. du Pont de Nemours and Company, Experimental Station, Wilmington, DE 19880-323, USA*

Received 29 August 2001; accepted 6 November 2001

Abstract

The peculiarities and kinetics of segmental dynamics in semi-crystalline poly(oxymethylene) (POM) were studied over the temperature range from 130 to 430 K, covering three broad relaxation regions, using DSC and laser-interferometric creep rate spectroscopy (CRS). A number of dynamic anomalies are observed. These included a suppressed glass transition (T_g) with its transformation into a number of segmental relaxations below and above T_g, and the pronounced dynamic heterogeneity, with the dispersion of activation energies of segmental motion at elevated temperatures from 80 to 500 kJ mol^{-1}. The formation of double or triple folds was found indicating a predominant contribution of ''straightened out'' tie chains to the structure of disordered regions in isotropic POM. Discrete high-resolution CRS analysis showed that up to 10 creep rate peaks (kinds of segmental motion) constituted dynamics in POM interlamellar layers. All the anomalies observed could be treated in terms of the concept of common segmental nature of α and β relaxations in flexible-chain polymers; as the breakdown of intermolecular motional cooperativity due to nanoscale confinement effect, and as different constraining influence of crystallites on dynamics in the intercrystalline layers.

Keywords: Poly(oxymethylene); Dynamics; Relaxation spectra; Calorimetry

1. Introduction

Poly(oxymethylene) (POM) is one of the important engineering plastics. High chain flexibility and symmetry result in rapid crystallization, rather high crystallinity, and complex morphology in this polymer, that composes a complicated spectrum of molecular motions in this polymer. Quite a few publications on relaxations in POM are known [1–10], which manifested themselves within three temperature regions covering at low frequencies: (a) the temperature range from ca. 150 to 220 K (relaxation I); (b) the range of 250 ± 20 K (relaxation II); (c) the broad region, extending from 300–320 K to the temperatures of 420–430 K (relaxation III) close to basic melting range. Analysis of these literature data prompts us to divide them into the those of the acceptable facts and those need further investigation.

The most convincing facts were obtained, in our opinion, for assignment of relaxation II to ''purely amorphous'', cooperative glass transition in disordered

* Corresponding author. Fax: +7-812-2478924.
E-mail address: vbersht@polmater.ioffe.ru (V.A. Bershtein).

0040-6031/02/$ – see front matter
PII: S0040-6031(02)00186-7

regions [3,4,6–8]. Assignment of T_g in POM has been controversial in the earlier literature. The relaxation I has been considered as the glass transition because of its relatively large height of loss peak [1] or of some heat capacity data [5], or due to abrupt change in the thermal expansion coefficient at the relevant temperature [1].

Nevertheless, the experimental results in favor of assignment of relaxation II to "usual" glass transition have been considered. According to van Krevelen [11], the hypothetical, "purely amorphous" $T_g = 223$ K at 10^{-3} Hz of POM that corresponds close to the relevant temperature position (~250–260 K) of the mechanical loss peak for relaxation II in quenched POM at 1 Hz [1], or to dielectric peak at ca. 290 K at 10^4 Hz [8]. Besides, relaxation peak II was enhanced at lowering of POM crystallinity and in POM blends [1]. While relaxations I and III were relatively invariant to diluents (10% additives), the relaxation peak II shifted considerably in the blends [7,8]. Typically cooperative, high effective activation energies of this relaxation, $Q_{II} \approx 170$ kJ mol^{-1} in POM or 240–280 kJ mol^{-1} in POM blends [7], also testified in favor of the assignment of relaxation II to glass transition. Large-scale interlamellar slip occurred in POM starting from the region of the relaxation II only that is also typical of glass transition [4].

At the same time, it is noteworthy that relaxation II turned out weak in POM. A few weeks of aging of quenched POM at room temperature depresses the intensity of relaxation II [1], down to its total disappearance in the mechanical loss spectrum [7]. It means that only small fraction of POM segments, located in the interlamellar disordered layers, remained undisturbed by crystallites and contributed to "purely amorphous" glass transition.

Less definite information has been obtained for relaxation I. Mechanical or dielectric relaxation peaks with the maximum at ca. 200 K were observed [1,3,7,8]. The mechanical losses increased in fact starting from ca. 100 K. The authors [3] observed two overlapping peaks, at 206–208 and 170–180 K (1–3 Hz), in POM mechanical loss spectra. Some complexity of the relaxation peak I is expected also from the TSDC spectral contour [8]. Different values of activation energies were obtained for this relaxation including non-cooperative (zero activation entropy ΔS_{act} [12]) magnitude of $Q_I \approx 50$ kJ mol^{-1}, and the values of ca. 100 kJ mol^{-1} [3,7,8]. This relaxation was associated presumably by different authors with motion of short segments in disordered regions or at lamellar surfaces, or with motion of defects inside the crystallites.

Of most significance is the dynamics in the broad temperature region of relaxation III. In this between T_g and T_m region, dynamics is undoubtedly associated with the presence of crystallites, and its characteristics in highly crystalline polymers depend on annealing regime, lamellar crystallite thickness, and crystallinity [1,13,14]. We believe that the dynamics in this temperature region for POM needs further investigation, as the data published and the interpretations offered are insufficient and contradictory in some aspects. It was recently indicated that dynamics in this temperature area in POM was not well understood [7].

It was assumed that "unfreezing" of segmental mobility at these temperatures has been explained by translational motions along a chain axis inside crystallites [2]. The authors [5] presumably assigned a slight endothermic effect, observed for molded POM as low as from ca. 320 K, to early melting of the smallest and/or defective crystallites (premelting process). Moreover, they estimated POM crystallinity by integrating of the endotherm starting from 320 K [5]. Thereto, position of the broad mechanical loss peak in this region was not affected by diluents in POM/diluent miscible blends that might testify in favor of intracrystalline origin of transition being considered [1,7].

Meantime, some other data indicate basically out-of-crystalline origin of dynamics in the ca. 300–400 K range. Thus, it was shown that heat capacity in this temperature range is not the sum of crystallite heat capacity and amorphous heat capacity multiplied with the appropriate weight fractions [5]. The negative deviations of POM heat capacity over this T_g–T_m range (as compared to heat capacity expected from two-phase model) were observed and treated as a consequence of a large role of "rigid amorphous fractions" [5]. There is also a close viewpoint that crystallite/amorphous interface species dominate in the disordered parts of POM [7,8]. In this case, just the "rigid amorphous fraction" is considered as giving the basic contribution to non-crystalline species in POM. Then, segmental motion within narrow (ca. 5 nm [15]) interlamellar layers of POM is affected (constrained) by crystallite surfaces [8]. That allows to suppose that motion of the majority of segments in POM disordered regions contributes not to the lower-temperature glass transition but to relaxation III.

Interestingly, the activation energies of segmental motion in this region, Q_{III}, in POM, obtained by different authors, indicated fivefold discrepancy in the values which were equal to 80, 84, 92, 105, 155, 210, 273 or 386 kJ mol^{-1} [1,6,7,9,10]. The cause of such large discrepancy has not been resolved for POM so far. However, it should be noted that all these values are typically relaxation mode, and do not indicate the dominant role of melting phase transition in this temperature range.

Finally, two comments can be made concerning the above arguments in favor of intracrystalline origin of relaxation III. First, there are theoretical predictions [16] admitting exclusion of polymer diluents not only from crystallites but also from the interfacial region, i.e. domains of "rigid amorphous species" [5,7,8]. Besides, the early endothermic effects on DSC curves cannot be considered as unconditional argument in favor of their assignment to melting of crystallites. As known, the endothermic peaks may be observed even for annealed non-crystalline polymers as a consequence of reduced enthalpy of a sample and "unfreezing" of motion in more densely packed domains [17].

The objective of this work was clarifying of the peculiarities of dynamics in semi-crystalline POM over the temperature range from ca. 100 to 420 K via detailed analysis by combined using of DSC and laser-interferometric creep rate spectroscopy (CRS).

2. Experimental

2.1. Samples

Du Pont POM (Delrin®) with $M_n = 66.000$ and narrow molecular weight distribution was studied. The samples contained less than 2% of the thermal stabilizer and antioxidant, and were obtained by injection molding, under pressure of 1000 bar, with cooling at the rate of ca. 200 K min^{-1}. The samples were aged by storage for 1 year before the measurements. Special treatments of the samples were used as described below.

2.2. DSC analysis of segmental dynamics

DSC curves were measured over the temperature range from 100 to 480 K using the Perkin-Elmer DSC-2 apparatus calibrated with water (273.1 K), cyclohexane (279.6 K), and indium (429.8 K). The heat capacity scale was calibrated using sapphire. The experiments were carried out under nitrogen or helium atmosphere. The heating rates of $v = 0.31$, 0.62, 2.5, 5, 10, 20 or 40 K min^{-1} were used; the standard rate was 10 K min^{-1}.

The samples with the identical masses of $m = 28 \pm 2$ mg and geometry ($4 \times 4 \times 1$ mm^3), with flat and smooth lower surface, were used. For correct characterization of heat capacity steps in slight low-temperature relaxations, very large samples of $m = 130$ mg (without a capsule) were also analyzed. The samples in their initial, aged state or after annealing under different conditions, or after fast cooling from melt in a calorimeter, or quenched from 423 K into liquid nitrogen, were studied. For compensating of non-specific heat capacity change with temperature, the silica glass was set in many experiments into the reference chamber of a calorimeter.

The temperature range under study covered the regions of relaxations I–III and melting transition range. For characterization of segmental dynamics below melting range, the following magnitudes were determined:

1. the temperature $T_{1/2}$ recorded at the half-height of the heat capacity step ΔC_P;
2. the onset, T_1, and completion, T_2, temperatures of the ΔC_P step, and transition range $\Delta T = T_2 - T_1$;
3. the values of the ΔC_P step and (in separate cases) the heat capacities C_P just before and after this step;
4. the effective activation energy Q of segmental motion as a function of temperature over a wide temperature range of relaxations I and III, i.e. around 200 K and at ca. 300–430 K;
5. the scale of motional unit event (Donth's volume) for relaxation I;
6. the degree of intermolecular cooperativity Z of segmental motion in glass transition (relaxation II).

As shown below, depending on POM thermal prehistory, DSC curves exhibited the ΔC_P steps, i.e. the distinct glass transition-like behavior, at various temperatures, from ca. 300 to 430 K. Besides, relaxation I at ca. 200 K could be characterized in detail. It allowed to single out and characterize a set of the

segmental motion modes prevailing at corresponding temperatures.

The effective activation energies were determined by displacement of the most distinct characteristic temperatures, T_1 or $T_{1/2}$, or T_2, with heating rate for any ΔC_P step. Typically, a series of identically annealed and cooled after treatment ($v = 320$ K min^{-1}) samples were used in each case, where each sample was heated with one rate. Under DSC time conditions, i.e. within rather narrow range of equivalent frequencies of 10^{-2}–10^{-1} Hz, the $\ln v$ versus T^{-1} plots obtained turned out to be linear. That permitted to estimate Q values and then $Q(T)$ dependence by the formula [17]:

$$Q = -R\frac{\mathrm{d}\ln v}{\mathrm{d}(T^{-1})} \tag{1}$$

The Donth's volume, as the scale of motional unit event [18], was determined for relaxation I by the formula:

$$V_\mathrm{D} = \frac{kT_\mathrm{tr}\Delta C_P^{-1}}{\rho(\delta T_\mathrm{tr})^2} \tag{2}$$

where $\Delta C_P^{-1} = \Delta C_P/C_P(T < T_\mathrm{tr}) \times C_P(T > T_\mathrm{tr})$; ρ is the POM density; $C_P(T < T_\mathrm{tr})$ and $C_P(T > T_\mathrm{tr})$ the heat capacities just before and after the ΔC_P jump at transition temperature T_tr; $\delta T_\mathrm{tr} = (T_2 - T_1)/2$ the half-width of the transition range measured on cooling from well above T_tr with a rate of 5 K min^{-1}; k the Boltzmann constant.

The accuracy of T, ΔC_P, Q, and V_D determinations was equal to ±1 K, ±5%, ±10–15%, and ±30%, respectively. The magnitude of parameter Z at T_g (relaxation II) was estimated as the ratio of Q_II, obtained earlier by DMA [7], to Q_I value obtained by DSC in this research (see Section 4).

Besides, DSC was used also for comparative estimates of melting parameters that allowed to obtain non-trivial information on conformational state of tie chains in the intercrystalline regions by estimation and comparing of lamellar crystallite thickness, l_c, and so-called "parameter of intrachain cooperativity of melting" v_m.

To perform the precise quantitative analysis, true melting point, T_m^t, and true melting range, $\Delta T_\mathrm{m}^\mathrm{t}$, were estimated. As known [17], three melting points are distinguished:

(1) the comparative characteristics, T_m, obtained at given heating rate;
(2) the true melting point, T_m^t, characterizing melting of crystallites with given structure and size;
(3) the equilibrium melting point, T_m^0, for a perfect, sufficiently large crystal where the role of free surface energy may be disregarded.

Normally, if the crystal structure is stable and invariable on heating, $T_\mathrm{m} > T_\mathrm{m}^\mathrm{t}$ due to overheating effects caused basically by a thermal lag. A difference $\Delta T^* = T_\mathrm{m} - T_\mathrm{m}^\mathrm{t}$ is proportional to a heating rate v, the melting enthalpy ΔH_m, a sample mass m, and the thermal resistance R [17,19]:

$$\Delta T^* = (2m\Delta H_\mathrm{m} R v)^{1/2} \tag{3}$$

R is determined by thermal resistance of both the instrument and a sample itself, and depends also on the thermal contact of the latter with its holder (capsule). When using the samples of identical mass, geometrical form, and with flat, smooth lower surface contacting holder, $R =$ constant is attained, and $\Delta T^* = f(v)^{1/2}$, i.e. at $v \to 0$, $T_\mathrm{m} \to T_\mathrm{m}^\mathrm{t}$. Therefore, T_m^t and $\Delta T_\mathrm{m}^\mathrm{t}$ values were obtained by measuring the temperatures of the onset, maximum and completion of melting peak (as estimated by the triangle method, i.e. by endotherm located between two tangent lines, characterizing melting of the absolute majority of crystallites [17]) at different heating rates, and subsequent extrapolating of the linear $T(v)^{1/2}$ plots or linear sections of these plots to a zero heating rate.

By using the Thomson–Gibbs equation

$$T_\mathrm{m}^\mathrm{t} = T_\mathrm{m}^0\left(1 - \frac{2\gamma_i}{\Delta H_\mathrm{m}^\circ \rho_\mathrm{c} l_\mathrm{c}}\right) \tag{4}$$

crystallite thickness, l_c, was estimated. Here, free surface energy of the end faces of lamellar POM crystallites $\gamma_i = 49$ erg cm^{-2} [20], $T_\mathrm{m}^0 = 457$ K, the enthalpy of POM crystals $\Delta H_\mathrm{m}^\circ = 326$ J g^{-1} [20,21], and the density of the crystals $\rho_\mathrm{c} \approx 1.5$ g cm^{-3}.

Of special interest was estimation by DSC of parameter v_m by formula [17]:

$$v_m = \frac{2R(T_\mathrm{m}^\mathrm{t})^2}{\Delta T_\mathrm{m}^\mathrm{t}\Delta H_\mathrm{m}^\circ} \tag{5}$$

where R is the gas constant here. Parameter v_m is a minimal sequence (a number) of monomer units in stereoregular chain section (helix for POM), which passes at melting as a whole into disordered, coiled state.

The accuracy of DSC determination of l_c and v_m was equal to ca. 10 and 30%, respectively.

2.3. Creep rate spectra

CRS, as the original method of relaxation spectrometry and thermal analysis, was developed and has been successfully applied at Ioffe Institute [22–31] to the problems of: (a) precise deformation kinetics analysis; (b) studying of microplasticity; (c) detailed, discrete characterization of molecular motion in polymers and other materials; (d) nanoscale dynamic, physical and compositional heterogeneity. CRS method is based on precise measuring of low creep rates as a function of temperature (creep rate spectrum) by using a laser interferometer based on Doppler effect. The obvious CRS superiority in resolution and sensitivity to widespread relaxation spectrometry techniques has been shown in the above publications. In this research, the CRS setup, operating under uniaxial tension, was used which has been described elsewhere [25].

The time evolution of sample deformation was registered as a sequence of beats in an interferogram which beat frequency f yielded a creep rate:

$$\dot{\varepsilon} = \frac{\lambda f}{2I_0} \tag{6}$$

where $\lambda = 630$ nm is the laser wavelength, and I_0 an initial length of a sample. The samples with 1×5 mm^2 cross-section and 5 cm length were used in these experiments.

CR spectra were measured over the temperature range from 130 to 420 K. A sample was cooled down to 130 K, and a small tensile stress, much lesser than the yield stress, was applied to a sample for 1 min. It allowed to record a creep process as a series of beats in the interferogram. Then a sample was unloaded, heated with the rate of 1 K min^{-1} to a temperature 5 K higher, and was loaded again at the same stress. Again, the interferogram was registered, the sample was unloaded and heated, and so on. Total recovery of deformation occurred after unloading and during a subsequent 5 min heating. Typically, the multiple peaks of increased creep rates appeared on the creep rate versus T curves measured in the way described.

Under a low stress, creep is associated predominantly with local shear strains, and a creep rate decreases with time as the process proceeds. Therefore, besides a stress, the second experimental parameter, time from a moment of loading to a moment of measuring, was kept constant at measuring a creep rate spectrum. Time $t = 10$ or 30 s was taken typically to reach simultaneously the best accuracy and resolution. The correlative, equivalent frequency of the CRS experiments was equal to $f_{\text{corr}} = (2\pi t)^{-1} \approx 10^{-3}$–$10^{-2}$ Hz, i.e. their time conditions were close to those in the DSC experiments.

High sensitivity of CRS technique allowed to measure the creep rates of 10^{-8}–10^{-3} s^{-1} at low stress on the basis of deformation increment of ca. 0.01% (a few hundred nanometers) only at $T < T_g$ or about 1% at $T \geq T_g$. The instrumental accuracy of creep rate measuring in these computerized experiments did not exceed 1%. The appropriate stress was chosen experimentally as capable of inducing sufficient creep rates to be measured while also maintaining a high spectral resolution. Too high stress caused undesirable effects of some distortion and smoothing out of the spectral contour and even early rupture of a sample. Small deformations in the measurements allowed to keep isostructural state of a sample during the experiment. That was corroborated by total recovery of the initial creep rate after a reverse jump in a temperature.

3. Results

Fig. 1 shows the possible manifestation of relaxations I, II and III on the DSC curves of POM.

The small heat capacity step $\Delta C_P \approx 0.07$ J g^{-1} K^{-1} at ~200 K corresponds to relaxation I. Its displacement with heating rate (Fig. 2, upper plot) and using the formula (1) permitted to estimate the activation energy of this relaxation transition: $Q_I \approx 60$ kJ mol^{-1}. For Arrhenius, non-cooperative relaxations, the frequency of jumps of the kinetic units $f \approx 10^{13} \exp(-Q/RT)$ or Q (kJ mol^{-1}) $\approx T$(K) $\times$ (0.25 − 0.019 log f) [17], i.e. $Q \approx 0.29T$ at the equivalent frequency $f \approx 10^{-2}$ Hz of DSC experiments, and Q_I obeys this relation. Consequently, relaxation I may be considered as the event of non-cooperative motion of a chain segment.

The motional event scale, Donth's volume V_D, was determined by the formula (2) proceeding from the DSC data and POM density $\rho \approx 1.43$ g cm^{-3}, $V_D = 0.2$–0.4 nm^3. Since the monomer unit volume in POM

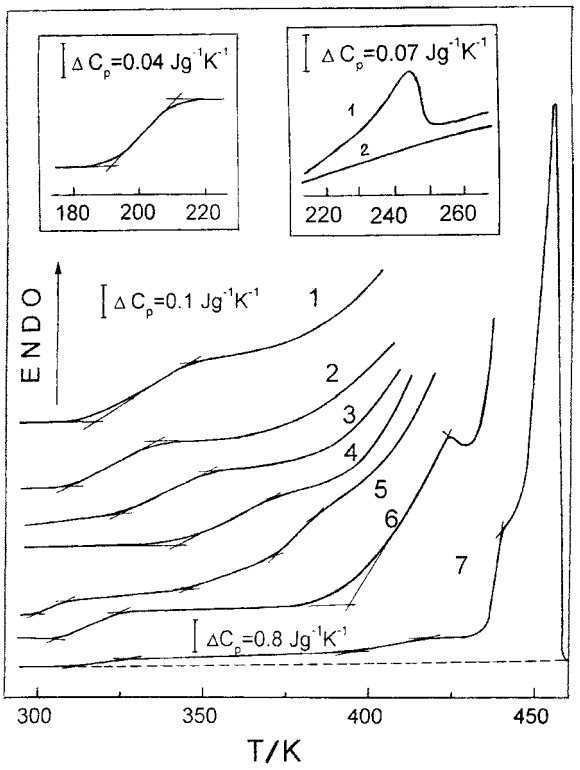

Fig. 1. DSC curves of POM in the initial aged state (1) and after cooling to 110 K with $v = 320$ K min^{-1} (the left inset), or after different thermal treatments; (2) for 3 h at 310 K after cooling from 500 to 300 K with $v = 320$ K min^{-1}; (3) for 2.5 h at 330 K, the same cooling regime; (4) for 0.5 h at 350 K, in the initial aged state; (5) for 1 h at 370 K, in the initial state; (6) for 3 h at 433 K plus 24 h storage at 293 K, after the indicated cooling; (7) for 3 h at 433 K plus 24 h storage at 293 K, in the initial state. The right inset: after quenching from 480 K into liquid nitrogen, scans 1 and 2. In all cases, heating rate $v = 10$ K min^{-1}. Cooling from annealing temperature to room temperature with the rate of 320 K min^{-1}.

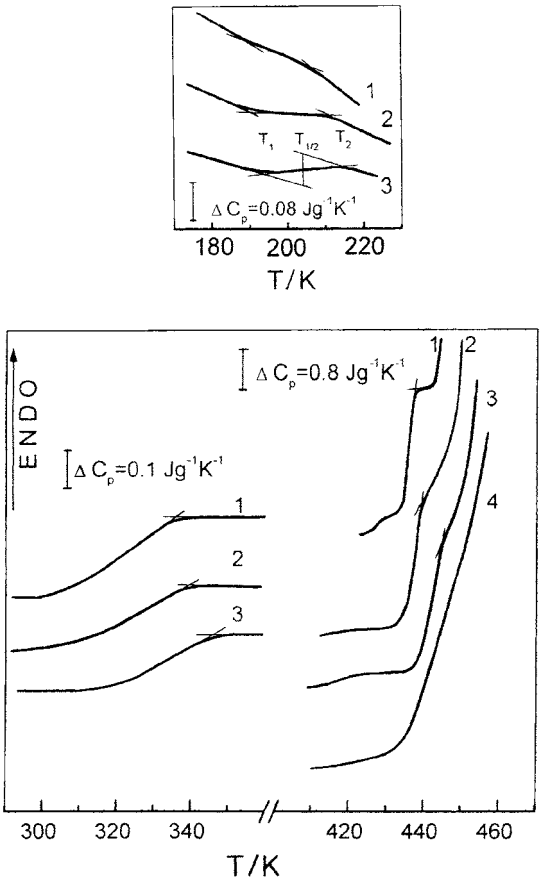

Fig. 2. DSC curves obtained at heating rates of 5 (1), 10 (2), 20 (3) or 40 K min^{-1} (4) for POM in the region of relaxation I, after cooling from 293 to 110 K with the rate of 320 K (above), and after annealing for 3 h at 310 K (below, on the left) or for 3 h at 433 K (below, on the right).

is equal to ca. 0.035 nm^3, it means that the moving segment in relaxation I includes 8 ± 3 monomer (CH_2–O) units, i.e. corresponds in length to statistical Kuhn segment (correlation length) in POM and many other flexible-chain polymers [17].

It shows that relaxation I has the same molecular mechanism as the β relaxation in non- or low-crystalline polymers (see Section 4). This conclusion is confirmed also by the $T_I/T_g = 0.77-0.80$ ratio, corresponding to regular Boyer's relation $T_\beta/T_g = 0.75 \pm 0.05$ [13], and by $Q_{II}/Q_I \approx 3$ ratio similar to the regular $Q_\alpha/Q_\beta = 4 \pm 1$ relation [17], where both relations are typical of flexible-chain polymers at low frequencies. It should be noted that relaxations I and II in POM are close, by their temperature position and other characteristics, to those in highly crystalline high-density PE. Meantime, for the latter, the indicated origin of relaxation I has been proved experimentally [17,32].

Suppressed glass transition (relaxation II) in POM could not be discerned by DSC as a rule in the samples studied, aged or annealed, or quenched in the calorimeter by cooling of melt with the rate of 320 K min^{-1}. Nevertheless, some heat capacity "anomaly" in this temperature region was found in our experiments for the samples quenched from melt into liquid nitrogen,

with immediate (for ca. 2–3 s) transfer of a sample into the calorimetric chamber cooled to 220 K. In this case, an increased POM heat capacity at 220–250 K and its sharp decrease at 250–260 K were observed at the first scanning. This ''anomaly'' was absent on the DSC curve at the second scanning (see the right inset in Fig. 1). Such manifestation of glass transition on the DSC curve is not typical of polymers. It resembles manifestation of glass transition in metallic glasses, where it is not easy to discern a heat capacity step at T_g but a distinct exotherm of structural ordering starts normally at this temperature. Heat capacity drop in intensely quenched POM at ca. 260 K was associated, obviously, also with some structural ordering starting from the moment of ''unfreezing'' of cooperative motion. It was however difficult to estimate accurately the activation energy of relaxation II by DSC ($Q_{II} \approx 170$ kJ mol^{-1}, by our DMA data [7]).

Thus, weak relaxations I and II may be assigned to usual, non-cooperative or intermolecularly cooperative, segmental relaxations, respectively. These are evidently free from the influence of crystallites as rigid constraints. As it follows from the CRS data given below, relaxations I and II are realized, really, within the intercrystalline layers; however, their partial contribution to POM segmental dynamics is very small.

Unlike that, the DSC data obtained testify in favor of the idea of the relaxation region III, extending from 280 to 300 to 420–430 K, as the process of gradual ''unfreezing'' of segmental motions, differently constrained by crystallites, in various molecular elements of the intercrystalline regions.

By using the samples in their initial aged state or after melting in the calorimeter, mostly with subsequent annealing at different temperatures, one could observe the distinct heat capacity steps on the DSC curves. On the whole, the ΔC_P steps could be ''created'' at any temperature over the temperature range investigated, from ca. 300 to 430 K. One or two, or even three such glass transition-like anomalies could be obtained on each curve (Fig. 1). Consequently, varying of the sample prehistory allowed us to single out and, then, to characterize a subsequent set of segmental motion modes, constituting the region of relaxation III, as a function of temperature. Each ΔC_P step corresponded to ''unfreezing'' of motional mode prevailing just in this narrow temperature range. Fig. 1 shows that an annealing temperature predetermined roughly the temperature location of basic heat capacity step on the DSC curve; however, a few steps could be observed sometimes on the DSC curve of annealed POM (curve 7).

Effective activation energy of segmental motion Q_{III} as a function of temperature was determined. In each experiment, four identical capsulated samples of the same mass (ca. 30 mg) and geometry (tablets of 1 mm thickness) underwent the identical treatment. Then, DSC curves were obtained for this series of samples at different heating rates. Activation energy values were determined by displacement of the most distinct temperatures of the heat capacity step (of its onset or half-height, or completion) with heating rate, by the formula (1).

Fig. 2 shows the typical examples of such ΔC_P displacement for the steps located at ca. 300–340 and ca. 430–440 K. In the latter case, the step disappeared at heating rate of 40 K min^{-1} due to its merging with a melting peak. Fig. 3 represents two typical examples of the heat capacity step temperature (T_1, $T_{1/2}$ or T_2) versus ln v linear plots obtained for the annealed POM. In the upper plot, a close slope of these dependencies is observed that assumes the close Q_{III} values, i.e. negligibly slight dynamic heterogeneity in the given narrow temperature range. Contrarily, the large difference in the slopes of lines in the lower plot implies a large dynamic heterogeneity within the selected temperature range.

Fig. 4 shows the ''transition'' temperature versus ln v plots estimated for the whole broad region of relaxation III. Their various slopes imply non-monotonic alteration in the Q_{III} magnitude with temperature. This is really corroborated by the dependence, represented in Fig. 5. Besides the experimental points obtained for temperatures within the region of relaxation III, the point obtained for relaxation I and, additionally, the point for the glass transition (at ca. 260 K), taken from our DMA data [7], are also indicated here.

A large dynamic heterogeneity within the region of relaxation III is obvious, indeed, that can be associated with the variable influence of crystallites, as the rigid constraints, on molecular motion in disordered regions (see below). One can see that the $Q(T)$ dispersion obtained involves both non-cooperative segmental motions (when activation entropy $\Delta S_{act} = 0$) and

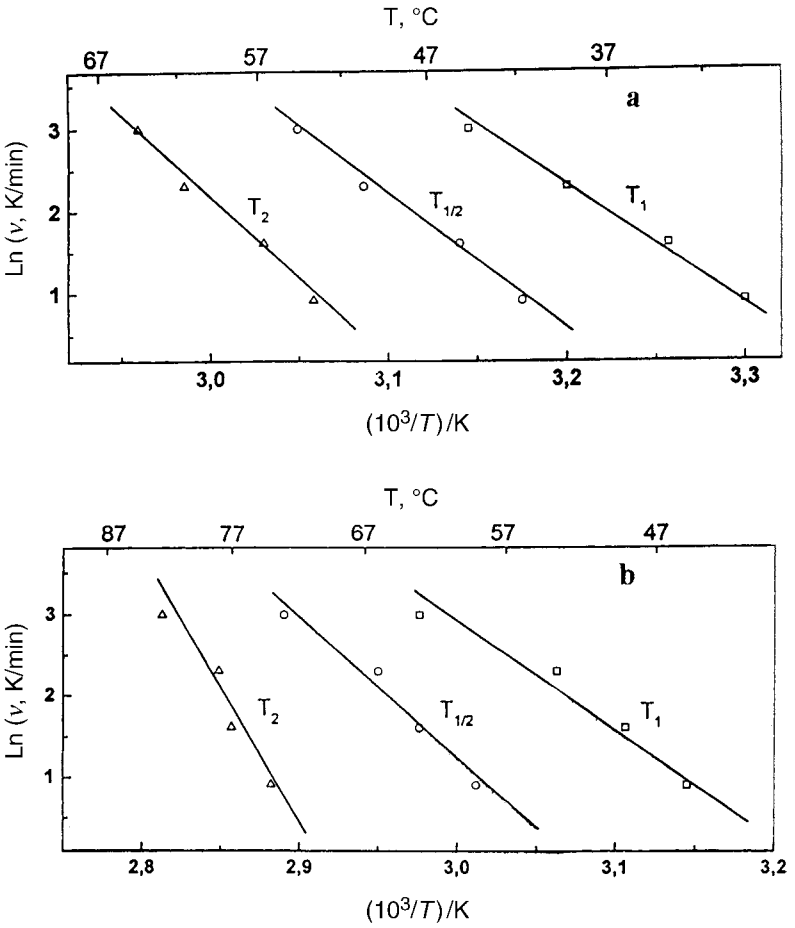

Fig. 3. Characteristic "transition" (heat capacity step) temperature versus ln ν plots for two typical steps found for annealed POM, illustrating the absence (a) or presence (b) of dynamic heterogeneity within the "transition" range.

the constituent relaxations differently deviating from the Arrhenius behavior. In a common case, such deviations may be a consequence of both enhanced constraining effect and motional cooperativity.

As indicated in Section 1, very different Q_{III} values have been obtained for POM by different authors by mechanical and dielectric relaxation techniques. A priori, such discrepancy could be related also to the difference in either a technique used or in the temperature range investigated. The basic cause for such enormous discrepancy remained obscure. Fig. 5 shows that the large Q dispersion in the region of relaxation III is not an accidental but a regular physical phenomenon, and the set of Q_{III} values, ranging from 80 to 500 kJ mol^{-1}, is found.

The region III in POM is characterized in fact by five kinds of relaxation behavior:

(1) almost "undisturbed", non-cooperative segmental motion just above T_g, near 300 K;
(2) less or moderately constrained segmental dynamics, with increasing deviation from the Arrhenius behavior, at ca. 340 K;
(3) strongly constrained segmental relaxations at ca. 360–380 K, when the activation energy turned out higher (250 kJ mol^{-1}) than that for unconstrained cooperative motion in the glass transition (ca. 170 kJ mol^{-1} [7]);
(4) a gradual decreasing, down to total disappearance, of the constraining effect and motional

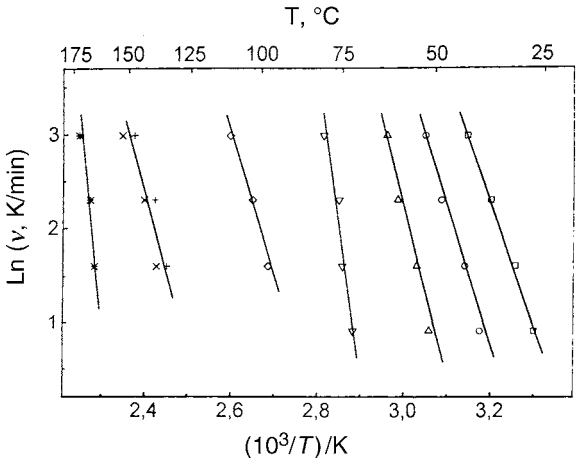

Fig. 4. A few heat capacity step temperature versus ln v plots obtained for POM at different temperatures of relaxation region III. Different slopes of the dependencies correspond to the complicated $Q(T)$ dependence in Fig. 5.

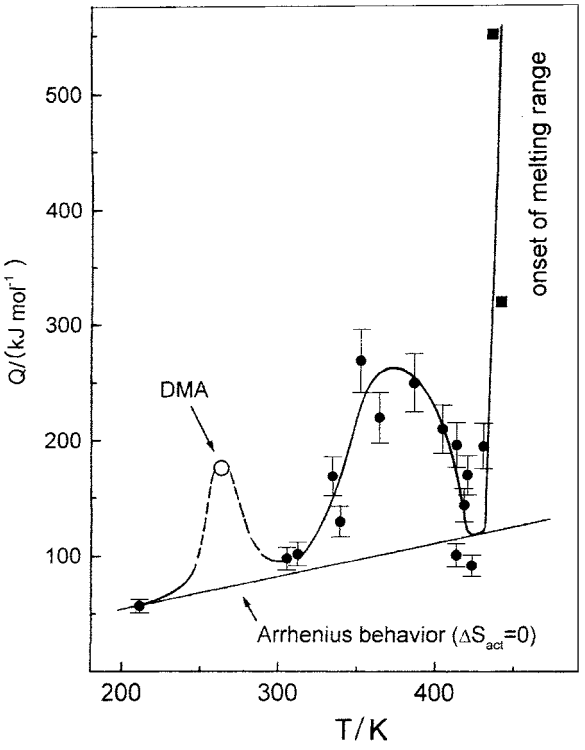

Fig. 5. Activation energy of segmental motion in POM as a function of temperature. One point obtained by DMA [7] is also given. Inclined straight line corresponds to Arrhenius relation at frequency of $\sim 10^{-2}$ Hz.

cooperativity, with Q dropping down to 80 kJ mol^{-1}, at 400–420 K;

(5) a very steep Q rise at 440 K, in the vicinity of the basic melting range, as a result of increasing role of this phase transition, for which formally Q aspires to infinity.

As discussed below, these specific changes in dynamics at elevated temperatures may be understood in terms of different conformational state of tie chains, interfacial behavior and the influence of ''softening'' of rigid constraints. It should be noted that this Q versus T dependence testifies in favor of the dominant contribution of relaxation (not phase) processes to dynamics over the range from ca. 300 to 420 K.

The interesting, independent information on the dominant state of tie chains in POM was obtained from the melting characteristics and then from the CRS data.

Fig. 6 gives the examples of melting peaks obtained for POM at three low heating rates. The POM crystallites were metastable that was noted earlier [20]. The doublet melting peak is observed under these conditions, and the height and temperature of the new, second peak increased with decreasing a heating rate. This indicates reorganization or/and recrystallization processes occurring in POM crystallites.

Fig. 7 shows the melting characteristic temperatures versus $v^{1/2}$ plots. The temperatures were determined from the endothermic peak as estimated by triangle method. One can see the independence of the temperature of peak onset of a heating rate. In accordance with Eq. (3), the true melting points, T_m^t, and true melting temperature ranges, ΔT_m^t, were obtained by extrapolating of the linear plots or the linear parts of these dependencies, obtained at $v = 2.5-10$ K min^{-1}, to $v = 0$. The magnitudes estimated are given in Table 1. Rather small width of the true melting range (ca. 2 K) should be noted here. It is clear that the upper limit for possible manifestation of relaxation III may attain ca. 440 K.

By using Eq. (4), the lamellar crystallite thickness l_c in POM was determined, which turned out to be equal to ca. 8 nm. This magnitude totally coincided with the l_c value estimated for molded POM by SAXS (the long period L and amorphous layer thickness l_a values [15] are also given in Table 1). This coincidence directly confirms the supposition that melting of the absolute

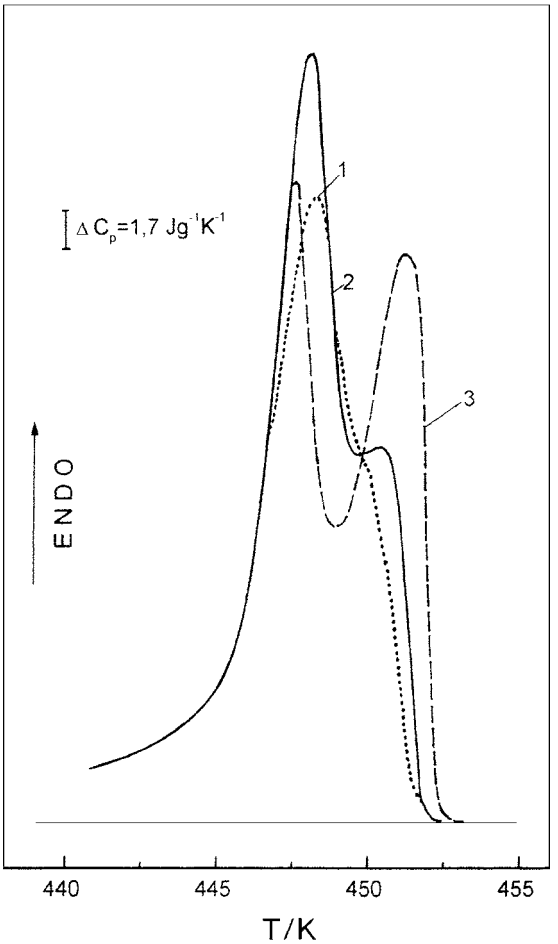

Fig. 6. Melting peaks obtained for three aged POM samples at heating rates of 1.25 (1), 0.62 (2), or 0.31 K min^{-1} (3).

majority of lamellae occurs really within the very narrow temperature range $\Delta T_m^t \approx 2$ K.

At the same time, the value of parameter v_m, estimated by Eq. (5), which was typically close to l_c in isotropic PE [17,33], turned out to exceed l_c in POM by far, and $v_m \approx 30-40$ nm (Table 1).

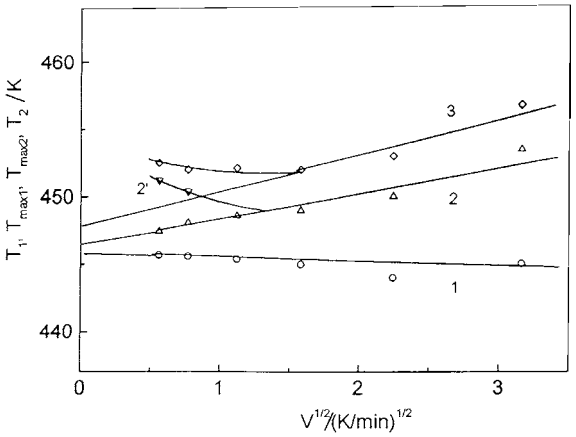

Fig. 7. Melting characteristic temperatures of the peak onset (1), maximum (2), and completion (3) versus heating rate obtained for the series of aged POM samples. The points 2′ are related to a new melting peak arising at low heating rates.

Large discrepancy between the v_m and l_c values was found earlier for the oriented polyethylene where $v_m \gg l_c$ [17,34,35]. The latter showed that very long *trans*-sequences of monomer units in chains prevailed in the structure of oriented PE, where each of them inevitably passed consecutively through a large number of crystallites and intercrystalline regions. At the temperature T_m^t, such *trans*-sequence passes as a whole from the straightened state into a random coil.

Analogously, the good conformity l_c^{DSC} and l_c^{SAXS} values in POM, and the obvious discrepancy between l_c and v_m magnitudes (Table 1) allowed to suppose that the found values of $v_m \approx (L + l_c)$ or $(2L + l_c)$ indicate the presence of a high content of ''double folds'' or ''triple folds'' in POM isotropic structure, where regular helical sections of chains extend through two or three lamellae. It is clear that such effect requires stereoregular helical (''straightened out'' or only slightly bent) state for the majority of tie chains in isotropic POM. That results in a conclusion of the

Table 1
POM: comparing of melting parameters and other characteristics, obtained therefrom, with SAXS/AFM structural parameters

DSC data						SAXS [15]			AFM [15], L (nm)
T_m^t (K)	$(T_m^t)_1$ (K)	ΔT_m^t (K)	v_m		l_c (nm)	l_c (nm)	l_a (nm)	L (nm)	
			Monomer units	nm					
446	445	2.2 ± 0.5	153 ± 35	35 ± 8	8 ± 0.5	8–9	4–5	12–14	24 ± 4

dominant contribution of strongly constrained tie chains to dynamics of intercrystalline layers in POM. The CRS data given below do not contradict this idea.

In this relation, the estimates of POM lamellar parameters by atomic force microscopy (AFM) are of interest [15]. As one can see from Table 1, the values of a long period, measured by AFM, are substantially larger ($L \approx 22-24$ nm) than these estimated by SAXS ($L \approx$ 12-14 nm). The authors [15] assumed that it might be associated with the contribution of stiff interfaces and decreased crystallite/interlamellar layer contrast.

Thus, the above DSC data provided the interesting information indicating a large dynamic heterogeneity in disordered regions of semi-crystalline samples studied. These give also some backgrounds for tentative assignment of the constituent relaxations being expected. Nevertheless, the real discrete analysis of the latter could be performed by CRS only.

Fig. 8 shows the CR spectra of POM obtained under tension and different experimental conditions (σ, t). Fig. 9 demonstrates spectral reproducibility for two identical aged POM samples, and besides allows to compare CR and mechanical loss spectra. A new sample was taken in each case.

Unlike the smooth mechanical loss contour with two, low- and high-temperature, broad relaxation peaks, the CR spectra are characterized by the complicated form; a few discrete or, more frequently, overlapping constituent peaks are observed. The peaks with the maxima, or manifesting themselves as contour nonmonotonies, such as steps or ''shoulders'' upon the edges of the larger neighboring peaks, are observed. The spectral contours consist of about 10 constituent peaks with various intensities which are located at approximately 150–170, 180–190, 200–210, 220–230, 250–260, 280–290, 320–340, 360, 380, and 400 K.

Fig. 8 indicates the significance of a correct choice of the experimental conditions to obtain an appropriate spectrum. First of all, it was impossible to use one stress magnitude over the whole temperature range under investigation (130–420 K), because of very different creep resistance at low temperatures and near melting range. Thus, too low stress (0.6 MPa) was not

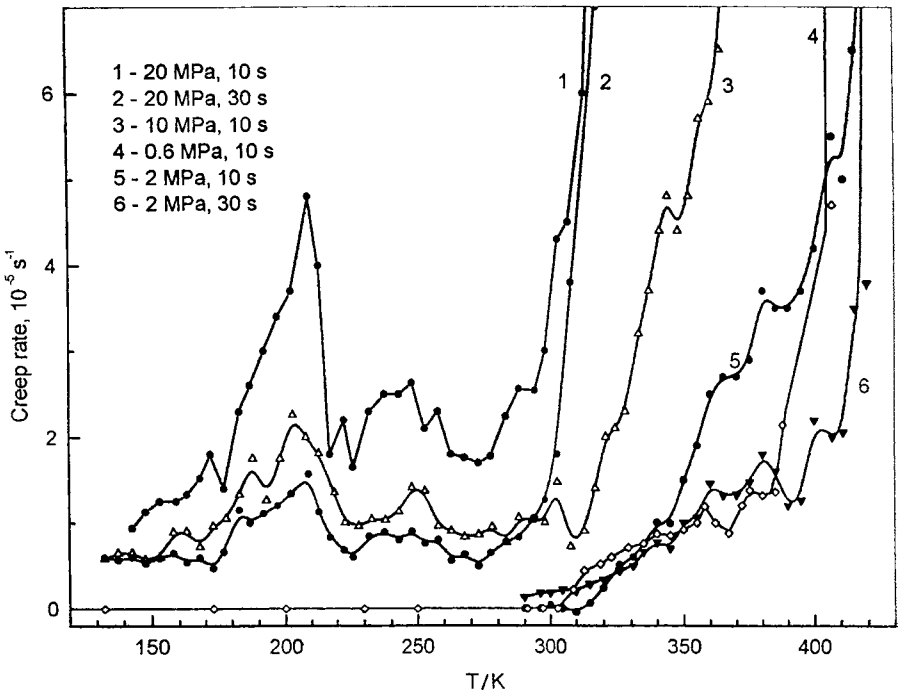

Fig. 8. CR spectra of POM obtained under tension and indicated experimental conditions (σ, t).

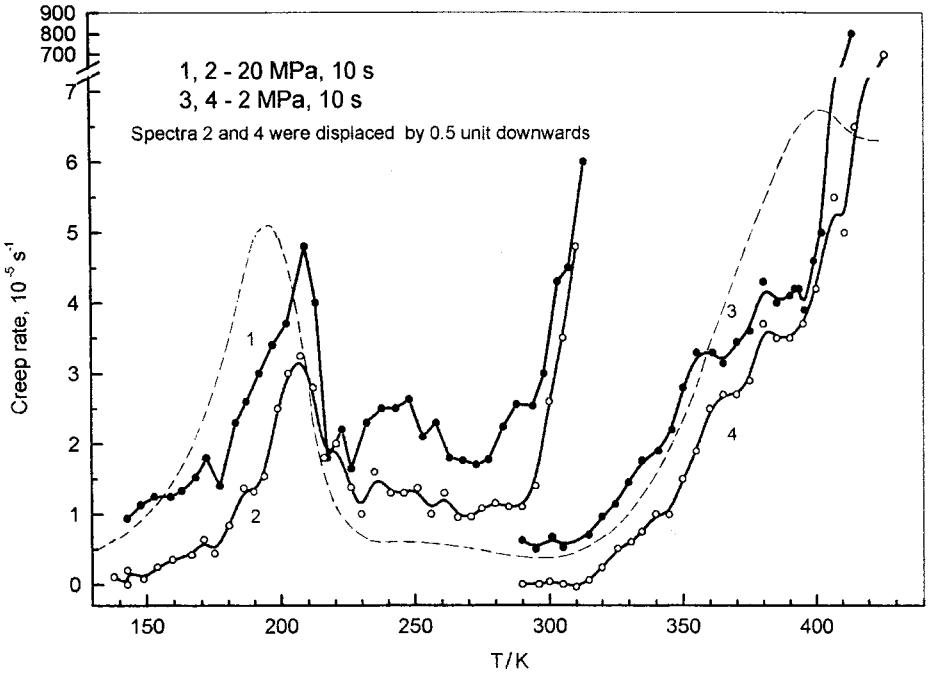

Fig. 9. CR spectra obtained for two identical POM samples under tension and indicated conditions, and illustrating the degree of spectral reproducibility. Dashed line corresponds to the contour of POM mechanical loss spectrum [1].

capable of inducing the sufficient creep rates below 300 K, whereas $\sigma = 10$ or 20 MPa provided the contrasting spectra at negative temperatures but was excessive at elevated temperatures. In the latter case, very steep rise of creep rates was observed, which was accompanied by smoothing out and distortion of a spectral contour, and arising of irreversible (at given temperature) plasticity, up to early sample rupture. Large accelerating of creep, by two orders of magnitude, occurred at ca. 420 K even under tensile stress of 2 MPa (Fig. 9).

Therefore, the standard experimental conditions chosen were as follows: 20 MPa and 10 s for the temperatures below 300 K, and 2 MPa and 10 s for elevated temperatures.

Fig. 9 shows satisfactory reproducibility of the CR spectra. Really, despite small difference in both CR spectra, approximately the same set of constituent relaxations, and the similar relative intensities of CR peaks (partial peak contributions to a spectrum) are reproduced in both spectra.

The above DSC data, together with some published data, allowed us to make the tentative assignments to constituent CR (relaxation) peaks in the POM spectrum, in accordance with their temperature location at the equivalent frequency of 10^{-3}–10^{-2} Hz (Table 2). First of all, because of much more malleableness of interlamellar layers as compared to rigid crystallites, the CR peaks 1–10, constituting the relaxation regions I, II and III, must be assigned to "unfreezing" of separate kinds of segmental motion in disordered, interlamellar layers.

CR peaks at ca. 150–210 K have to be related to non-cooperative Kuhn segment motion (relaxation I, cooperativity degree $Z = 1$), similar to the β relaxation in non- or low-crystalline polymers. Unlike a single mechanical loss peak in this region [1,7] (doublet peak was observed only in the work [3]), the triplet is observed in the CR spectrum in this region where peak at 210 K is the basic one. As follows from the above, the relevant segmental motions may occur at the sites of loosened molecular packing, for chain sections, non-disturbed by crystallites. Peaks 1, 2 and 3 indicate some dynamic heterogeneity in this temperature range. It is not surprisingly because of complicated conformational structure of some chains in

Table 2
Distinct creep rate peaks in the POM spectrum obtained under tension[a]

Peak no.	T (K)	Relative intensity of the peaks[b]	Tentative assignment of the peaks characterizing "unfreezing" of segmental motion within the intercrystalline regions (compare with $Q\{T\}$ dependence in Fig. 5)
1	150–170	+	Non-cooperative relaxation I ($Z = 1$), similar to the β relaxation in non- or low-crystalline polymers, and its dynamic heterogeneity
2	180–190	+	
3	200–210	◆	
4	220–230	+	Relaxation region II: intermediate relaxation ($Z = 2$)
5	250–260	+	Relaxation region II: cooperative glass transition ($Z = 3$)
6	280–300	+	Relaxation region III: slightly constrained segmental motions
7	320–340	+	Relaxation region III: slightly constrained segmental motions
8	350–360	◆	Relaxation region III: strongly constrained segmental motions
9	380	◆	Relaxation region III: strongly constrained segmental motions
10	~400	◆	Segmental motion in the most constrained chains after "softening" of crystalline constraints

[a] The experimental conditions: 20 MPa and 10 s at temperatures below 300 K, and 2 MPa and 10 s above 300 K.
[b] The discrete or partly overlapping peaks are considered including the maxima or steps, or "shoulders" in the spectral contour. Signs + and ◆ designate a slight peak or a pronounced peak, respectively.

interlamellar layers. Moreover, nanostructure-sensitive dynamic heterogeneity in the β relaxation has been shown earlier by CRS even for simple non-crystalline polymers such as PMMA [23], PVC [26], or polycarbonate (four CR peaks at 130–230 K) [31].

In the region of 230–260 K, DMA [7] and DSC showed strongly suppressed, very slight glass transition (relaxation II), which was practically absent in POM after its long aging. Unlike that, Figs. 8 and 9 show small overlapping CR peaks at 220–260 K corresponding apparently to "intermediate", low-cooperative ($Z = 2$) segmental relaxation (220–230 K) and cooperative glass transition ($Z = 3$) at ca. 250–260 K (peaks 4 and 5 in Table 2). Again, it should be mentioned that just CRS allowed earlier to observe discretely these both relaxations in polymer system (Fig. 4 in [25]).

Thus, peaks 1–5 can be assigned to "usual" Kuhn segment motions with different intermolecular cooperativity degree, which are not underwent, obviously, to appreciable influence of crystallites. Such situation may be realized in POM, having very narrow intercrystalline layers with the thickness of 4–5 nm [15], with difficulty and only for a small fraction of segments. Judging by the relative heights of CR peaks in a spectrum at constant stress, the partial contribution of low-temperature CR peaks into POM dynamics is really extremely small, anyway, less than 10%.

The CR peaks 6–10 cover the broad temperature region of relaxation III, and relate to motions which play, undoubtedly, the dominant role in segmental dynamics in POM. Besides relatively slight peak at 280–300 K, much more pronounced, overlapping peaks at 320–340, 360, 380 and 400 K can be distinctly observed already at 0.6 MPa, when the other peaks could not be discerned at all (Fig. 8).

Comparing of the CRS data with Fig. 5 shows that CR peaks 7, 8 and 9 (Table 2) correspond to increasingly constrained segmental relaxations in disordered regions, with considerably increasing activation barriers to segmental motion. The constraining effect increases, evidently, with reduction in a degree of tie chains coiling, and in a distance between moving segment and chain attachment point at the crystallite surface.

Finally, CR peak 10 at ca. 400 K has to be assigned to "unfreezing" of segmental motion within the most constrained chains, e.g. "straightened out" tie ones (regular helix), or for segments directly attached to crystallite surface. The latter may be considered also in terms of "segments at interfaces". It is clear that segmental motion in such cases may start only if melting of the anomalously thin lamellae or/and "boundary melting" [36,37] of "normal" crystallites occur. In other words, this kind of segmental motion is indispensably associated with the effect of "softening" of rigid constraints. The latter was validated by

the above-mentioned sharp reduction of the activation energy of segmental motion at ca. 400 K (Fig. 5). Peaks 9 and 10 give the basic contribution to the CR spectrum that confirms the dominant role of ''straightened out'' and slightly bent tie chains in interlamellar layers of POM. This results is in a total accordance with the found inequality $\nu_m \gg l_c$ (Table 1).

4. Discussion

Thus, POM provides a good example of anomalous dynamics in the disordered regions of semi-crystalline polymer, when ''usual'' cooperative glass transition basically degenerates, transforming into a series of segmental relaxations, both below T_g (enhanced β and low-cooperative relaxations) and above T_g (differently constrained segmental relaxations over the T_g–T_m range). This ''anomalous'' dynamic behavior may be readily treated proceeding from the special state of chains in the intercrystalline layers, confined to nanoscale spaces and covalently anchored, from both ends, to crystallite surfaces as rigid structural constraints. Besides, the concept of common segmental nature of α and β relaxations in flexible-chain polymers has to be taken into account for interpretation of the results obtained.

Understanding of the latter may be found in framework of common, one of the challenging physical problems, viz., of anomalous dynamics around T_g under conditions of nanoscale confinement (finite-size effect), with strong interaction of confined substance with the restricting surface (constraining effect).

Last time, a large series of theoretical and experimental studies have been performed in this field, mostly for the substances in nanopores [38–44], nanoscale (5–100 nm) thickness polymer films [45–52], and for different complex polymer systems [25–29,53–66]. The dynamic anomalies, which have been observed in these studies, were as follows:

(1) considerable displacement of T_g to both lower and higher temperatures compared to that in ''free'' substances;
(2) multifold broadening of the glass transition range;
(3) partial breakdown of motional cooperativity or total transformation of cooperative glass (α) transition into non-cooperative β relaxation;
(4) large asymmetry of segmental relaxation dispersion at T = constant;
(5) arising of a large dynamic heterogeneity within the broad glass transition range, with a wide activation energy Q dispersion;
(6) large Q decreasing or increasing;
(7) partial or even total suppression of glass transition.

Some models have been proposed to account for the extraordinary breadth of glass transition and other anomalies in complex systems, in particular in single-phase, miscible polymer blends [67–69]. However, physical understanding of the above anomalies still remained incomplete up to last years because of a paucity of the direct experimental data. The latter gap has been filled up to a certain extent by the above (mostly DSC/CRS) studies performed for block copolymers [54,61], graft copolymers [55], miscible blends [27,60], polymer–silica hybrid materials [63], interpenetrating polymer networks [25,26], hybrid polymer–polymer networks [28,29], fullerene core star-like polymers [62,66], and molecular composites [65]. On this basis, the simple scheme was offered, explaining from the common grounds six kinds of the anomalous glass transition behavior in complex polymer systems [29,62].

Of importance for this approach is the experimentally proved concept of common segmental nature of α and β relaxations in flexible-chain polymers [17,70,71] which considers these relaxations as intermolecularly cooperative and non-cooperative motions, respectively, of Kuhn statistical segments; β relaxation event occurs at sites of loosened segmental packing (excess free volume) only. Amongst the found regular relations, connecting the activation parameters of α and β relaxations with molecular characteristics of polymers, it should be mentioned the ratio:

$$Z = \frac{Q_\alpha}{Q_\beta} \approx \frac{V_\alpha}{V_\beta} \approx \frac{V_D}{V_S} = 4 \pm 1 \quad (7)$$

where Z is a parameter of intermolecular cooperativity of segmental motion in the glass transition at low frequencies; Q_α, Q_β, V_α, and V_β the activation energies and activation volumes of α and β relaxations, respectively; V_D the motional event scale in the glass transition (Donth's volume); V_S the statistical segment volume.

Two opposite influences predetermine on the whole anomalous glass transition behavior in different cases of nanoheterogeneous systems, consisting of relatively ''soft'' polymer and rigid structural constituents:

1. Loosening of segmental packing in soft constituents, located in nanoscale-confined geometry. It may lead to a partial breakdown or even total collapsing of intermolecular cooperativity of segmental motion. In other terms, cooperative α relaxation $\rightarrow$ low-cooperative intermediate relaxation $\rightarrow$ non-cooperative β relaxation transformations may occur in this case. It is ''pure confinement effect'' when contribution of interactions between a polymer and a rigid constraint (rigid block, rigid macromolecule, inorganic nanophase, filler surface, etc.) is minor. Lower-temperature broadening of glass transition and decreasing of its parameters occurs under these conditions.
2. Covalent anchoring of chain segments to, or their strong non-chemical interaction with a rigid structural constituent. In this case, constraining influence of the latter on dynamics may dominate that increases the temperatures and activation barriers to segmental motion. This may occur, especially, at interfaces, for segments directly anchored to a constraint, and for strongly constrained, e.g. straightened out'' chains.

In some cases, these both effects were observed simultaneously, i.e. confinement effect prevailed for some segments whereas constraining one for others [29,65].

The similar dynamic behavior was also found for highly crystalline high-density PE, on the basis of combined DSC/NMR/X-ray diffraction studies, with studying also of etched samples with removed disordered component [17,32,72]. As found, relaxations I, II and III in PE, which are observed at temperatures close to these in POM (at 140–180, 240–270, and 300–370 K), were associated with segmental motion in the intercrystalline layers. Like that in POM, cooperative glass transition of ''amorphous species'' (relaxation II) was depressed transforming into both more pronounced lower-temperature, non-cooperative relaxation I, and differently constrained segmental relaxations III in the T_g–T_m region.

Thus, despite some differences observed in dynamics of HDPE and POM (which have to be analyzed separately), it is natural to consider a highly crystalline polymer as complex, nanostructured polymer system where lamellae are relatively rigid structural constraints (at $T \ll T_m$), while chains in the interlamellar layers are confined to nanoscale spaces and, additionally, are strongly anchored to these constraints.

Almost total ''degeneration'' of ''usual'' glass transition, enhancing of low-temperature non-cooperative relaxation, and gradual ''unfreezing'' of segmental dynamics at elevated temperatures in highly crystalline polymers (HDPE, POM, etc.) are a consequence of the specificity of the structure of intercrystalline layers, especially of different conformational state (coiling degree) of chains. Analysis of dynamics in PE interlamellar layers [17,72,73] showed that the step-like, gradual ''unfreezing'' of segmental mobility below T_m is determined by the ratio $y = l/h$, where h is a distance between the ends of tie chains or loops, and l their contour length. If the y is larger, the lower is the temperature of ''unfreezing'' of segmental motion. The distribution function for the parameter $y = 1.5-4$ was found for HDPE by NMR data [72,73].

It is clear that the regular helical tie chains, ''straightened out'' or slightly bent, and the segments of interfacial layer are most constrained by crystallites in POM. ''Unfreezing'' of segmental motion herein directly depends on phase transition of melting. As indicated, such tie chains just predominate in POM.

Large, threefold Q reduction in POM at 400–420 K, in the vicinity of basic melting range, is a new effect, which has not been discerned in PE [32], and it is apparently associated with some ''softening'' of rigid crystalline constraints. Two points may be responsible for such ''softening'': melting of the thinnest, anomalous POM lamellae at $T \geq 400$ K or/and boundary (partial, surface) melting of ''normal'' lamellae. According to Fischer's theory [36,37], excessive disorder and increased entropy at the crystallite surface give rise to boundary melting.

5. Conclusions

1. Combined DSC/CRS study of segmental dynamics in POM in very broad temperature range allowed the detailed, discrete analysis of segmental

relaxations constituting dynamics within intercrystallite regions of this polymer with complicated morphology.

2. Transformation of ''usual'' cooperative glass transition into low- and non-cooperative motions, and slightly or moderately, or strongly constrained segmental relaxations was observed. That predetermined large heterogeneity of segmental dynamics in POM as typical highly crystalline polymer. As found, the dominant contribution of ''straightened out'' or, may be, slightly bent tie chains to conformational state of intercrystallite layers in isotropic POM is observed, that predetermined the basic role of high-temperature, strongly constrained segmental relaxations in POM dynamics.
3. Similar to that for many other nanostructured polymer systems, all the peculiarities of dynamics in POM could be interpreted in framework of such common physical notions as anomalous dynamics in nanoscale-confined geometry; constrained dynamics; common segmental nature of α and β relaxations, and partial breakdown or total collapsing of motional cooperativity under certain conditions.

Acknowledgement

This work was supported by Du Pont and CRDF project RCO-889.

References

[1] N.G. McCrum, B.E. Read, G. Williams, Anelastic and Dielectric Effects in Polymeric Solids, Wiley, New York, 1967.
[2] M. Takayanagi, Mem. Fac. Eng. Kyushi Univ. 23 (1963) 41.
[3] R.J.V. Hojbors, E. Baer, P.H. Geil, J. Macromol. Sci.-Phys. B 13 (1977) 323.
[4] M.E. Kazen, P.H. Geil, J. Macromol. Sci.-Phys. B 13 (1977) 381.
[5] H. Suzuki, J. Grebowicz, B. Wunderlich, Macromol. Chem. 186 (1985) 1109.
[6] J.B. Enns, R. Simha, J. Macromol. Sci.-Phys. B 13 (1977) 25.
[7] M.Y. Keating, B.B. Sauer, E.A. Flexman, J. Macromol. Sci.-Phys. B 36 (1997) 717.
[8] B.B. Sauer, P. Avakian, E.A. Flexman, M.Y. Keating, B.B. Hsiao, R.K. Verma, J. Polym. Sci. B 35 (1997) 2121.
[9] R.W. Gray, J. Mater. Sci. 8 (1973) 1673.
[10] H.W. Starkweather Jr., Macromolecules 19 (1986) 2538.
[11] D.W. van Krevelen, Properties of Polymers, their Estimation and Correlation with Chemical Structure, Elsevier, Amsterdam, 1976.
[12] H.W. Starkweather Jr., Macromolecules 14 (1981) 1277.
[13] R.F. Boyer, J. Polym. Sci. Symp. 50 (1975) 189.
[14] R.H. Boyd, Polymer 26 (1985) 323, 1123.
[15] B.B. Sauer, R.S. McLean, D.J. Londone, J. Macromol. Sci.-Phys. B 39 (2000) 519.
[16] S.K. Kumar, D.Y. Yoon, Macromolecules 22 (1989) 4098.
[17] V.A. Bershtein, V.M. Egorov, Differential Scanning Calorimetry of Polymers, Physics, Chemistry, Analysis, Technology, Ellis Horwood, New York, 1994.
[18] E. Donth, J. Non-Cryst. Solids 53 (1982) 325.
[19] K. Illers, Eur. Polym. J. 10 (1974) 911.
[20] M. Jaffe, B. Wunderlich, Kolloid-Z.u.Z. Polymere 216–217 (1967) 203.
[21] B. Wunderlich, Macromolecular Physics, Vol. 3, Crystal Melting, Academic Press, New York, 1980.
[22] N.N. Peschanskaya, P.N. Yakushev, A.B. Sinani, V.A. Bershtein, Thermochim. Acta (Therm. Anal. Calorim. Polym. Phys.) 238 (1994) 429.
[23] N.N. Peschanskaya, P.N. Yakushev, A.B. Sinani, V.A. Bershtein, Macromol. Symp. 119 (1997) 79.
[24] N.N. Peschanskaya, P.N. Yakushev, V.Yu. Surovova, Phys. Solid State 37 (1995) 1429.
[25] V.A. Bershtein, P.N. Yakushev, L. Karabanova, L. Sergeeva, P. Pissis, J. Polym. Sci. B 37 (1999) 429.
[26] V.A. Bershtein, P.N. Yakushev, N.N. Peschanskaya, Macromol. Symp. 147 (1999) 73.
[27] V.A. Bershtein, L.M. Egorova, V.A. Ryzhov, P.N. Yakushev, Macromol. Symp. 149 (2000) 87.
[28] V.A. Bershtein, L.M. Egorova, V.A. Ryzhov, P.N. Yakushev, A.M. Fainleib, T.A. Shantalii, P. Pissis, J. Macromol. Sci.-Phys. B 40 (2001) 109.
[29] V.A. Bershtein, V.M. Egorov, L.M. Egorova, P.N. Yakushev, A.M. Fainleib, P. Pissis, P. Sysel, Proceedings of the Conference NATAS 2000, Orlando, p. 604.
[30] V.A. Bershtein, N.N. Peschanskaya, J.L. Halary, L. Monnerie, Polymer 40 (1999) 6687.
[31] V.A. Bershtein, N.N. Peschanskaya, P.N. Yakushev, Proceedings of the Conference NATAS 2000, Orlando, p. 482.
[32] V.A. Bershtein, V.M. Egorov, V.A. Marikhin, L.P. Myasnikova, Vysokomol. Soedin. A 27 (1985) 771.
[33] V.A. Bershtein, V.M. Egorov, V.A. Marikhin, L.P. Myasnikova, Vysokomol. Soedin. A 28 (1986) 1983.
[34] V.A. Bershtein, V.M. Egorov, V.A. Marikhin, L.P. Myasnikova, Vysokomol. Soedin. A 32 (1990) 2380.
[35] V.A. Bershtein, V.M. Egorov, V.A. Marikhin, L.P. Myasnikova, Intern. J. Polym. Mater. 22 (1993) 167.
[36] E.W. Fischer, Kolloid-Z.u.Z. Polymere 218 (1967) 7.
[37] E.W. Fischer, Pure Appl. Chem. 26 (1971) 385.
[38] C.L. Jackson, G.B. McKenna, J. Non-Cryst. Solids 131–133 (1991) 221.

[39] C.L. Jackson, G.B. McKenna, Chem. Mater. 8 (1996) 2128.
[40] P. Pissis, D. Daoukakis-Diamanti, L. Apekis, C. Christodoulides, J. Phys. Condens. Mat. 6 (1994) L325.
[41] Yu.B. Melnichenko, J. Schuller, R. Richert, B. Ewen, J. Chem. Phys. 103 (1995) 2016.
[42] W. Gorbatschow, M. Arndt, R. Stannarius, F. Kremer, Europhys. Lett. 35 (1996) 719.
[43] M. Arndt, R. Stannarius, H. Groothues, E. Hempel, F. Kremer, Phys. Rev. Lett. 79 (1997) 2077.
[44] A. Huwe, F. Kremer, P. Behrens, W. Schwieger, Phys. Rev. Lett. 82 (1999) 2338.
[45] J.L. Keddie, R.A.L. Jones, R.A. Cory, Europhys. Lett. 27 (1994) 59.
[46] J.L. Keddie, R.A.L. Jones, R.A. Cory, Faraday Discuss. 98 (1994) 219.
[47] W.E. Wallace, J.H. van Zanten, W.L. Wu, Phys. Rev. E 52 (1995) R3329.
[48] J.H. van Zanten, W.E. Wallace, W.L. Wu, Phys. Rev. E 53 (1996) R2053.
[49] G. Reiter, Europhys. Lett. 23 (1993) 579.
[50] Y.C. Jean, R. Zhang, H. Cao, J.-P. Yuan, C.-M. Huang, B. Nielsen, P. Asoka-Kumar, Phys. Rev. B 56 (1997) R8459.
[51] J.A. Forrest, K. Dalnoki-Verres, J.R. Dutcher, Phys. Rev. E 56 (1997) 5705.
[52] O. Brucker, S. Christian, H. Bock, C.W. Frank, W. Knoll, ACS Polym. Prepr. 88 (1997) 918.
[53] S. Krause, M. Iskandar, M. Igbal, Macromolecules 15 (1982) 105.
[54] V.A. Bershtein, V.Yu. Levin, L.M. Egorova, V.M. Egorov, et al., Vysokomol. Soedin. A 29 (1987) 2360, 2553.
[55] V.A. Bershtein, L.M. Egorova, L.I. Ginzburg, Vysokomol. Soedin. A 29 (1987) 2564.
[56] M. Aubin, R.E. Prud'homme, Polym. Eng. Sci. 28 (1988) 1355.
[57] J. Roovers, P. Toporowsky, Macromolecules 25 (1992) 3454.
[58] C.M. Roland, K.L. Ngai, Macromolecules 25 (1992) 363.
[59] B.B. Sauer, B.S. Hsiao, J. Polym. Sci. B 31 (1993) 917.
[60] V.A. Bershtein, L.M. Egorova, R.E. Prud'homme, J. Macromol. Sci.-Phys. 36 (1997) 513.
[61] V.A. Bershtein, L.M. Egorova, P. Sysel, J. Macromol. Sci.-Phys. 37 (1998) 747.
[62] V.A. Bershtein, V.M. Egorov, L.M. Egorova, P. Sysel, V.N. Zgonnik, J. Non-Cryst. Solids 235–237 (1998) 476.
[63] V.A. Bershtein, L.M. Egorova, P.N. Yakushev, G. Georgoussis, A. Kyritsis, P. Pissis, P. Sysel, L. Brozova, Macromol. Symp. 146 (1999) 9;
V.A. Bershtein, L.M. Egorova, P.N. Yakushev, G. Georgoussis, A. Kyritsis, P. Pissis, P. Sysel, L. Brozova, J. Polym. Sci. B 40 (2002) 1056.
[64] B.B. Sauer, N.V. DiPaolo, P. Avakian, W.G. Kampert, J.H. Starkweather Jr., J. Polym. Sci. B 31 (1993) 1851.
[65] V.A. Bershtein, L.M. Egorova, P.N. Yakushev, O. Meszaros, P. Sysel, L. David, A. Kanapitsas, P. Pissis, J. Macromol. Sci.-Phys. B 41 (2002) 419.
[66] V.A. Bershtein, V.M. Egorov, V.N. Zgonnik, E.Yu. Melenevskaya, L.V. Vinogradova, J. Therm. Anal. Calorim. 59 (2000) 23.
[67] K.L. Ngai, R.W. Rendell, J. Non-Cryst. Solids 131–133 (1991) 942.
[68] A. Jones, P.T. Inglefeld, Y. Lui, A.K. Ray, B.J.J. Caley, J. Non-Cryst. Solids 131–133 (1991) 556.
[69] E.W. Fischer, A. Zetsche, ACS Polym. Prepr. 33 (1992) 78.
[70] V.A. Bershtein, V.M. Egorov, L.M. Egorova, V.A. Ryzhov, Thermochim. Acta (Therm. Anal. Calorim. Polym. Phys.) 238 (1994) 41.
[71] V.A. Bershtein, V.A. Ryzhov, Adv. Polym. Sci. 114 (1994) 43.
[72] E.A. Egorov, V.V. Zhizhenkov, V.A. Marikhin, L.P. Myasnikova, A. Popov, Vysokomol Soedin. A 25 (1983) 693.
[73] E.A. Egorov, V.V. Zhizhenkov, V.A. Zakrevskii, Macromol. Chem. Macromol. Symp. 72 (1993) 47.